Development of a hybrid material based on Zn-Mg spinel ferrites covered with polypyrrole: structural, morphological, and electrical characteristics

M. G. Diop, M. Gueye , M. Lo*, D. Faye, M. Cisse, M. Guene
[a] *Organic and Physical Chemistry and Environmental Analysis Laboratory, Department of Chemistry, Faculty of Science and Technology, Cheikh Anta Diop University, Dakar, Senegal*

In this study, we synthesized a range of spinel ferrite $ZnxMg_{1-x}Fe_2O_4$ (x = 0, 0.3) forms using the sol-gel method. Additionally, polypyrrole nanosphere supported by magnesium and zinc ferrites ($ZnxMg_{1-x}Fe_2O_4$@PPy) were synthesized through in-situ polymerisation. The surfaces of $Zn_xMg_{1-x}Fe_2O_4$ (x = 0, 0.3) and $Zn_xMg_{1-x}Fe_2O_4$@PPy were subjected to spectroscopic analysis. The data obtained from X-ray diffraction (XRD) confirmed the formation of Zn-Mg spinel ferrite. The electrochemical analysis results demonstrated that the $Zn_{0.3}Mg_{0.7}Fe_2O_4$@PPy nanocomposites exhibited enhanced redox activity and a higher current intensity. This study highlights the development of hybrid $Zn_{0.3}Mg_{0.7}Fe_2O_4$@PPy type nanospheres with substantial and effective electrochemical properties, which could be a suitable option for industrial applications.

(Received April 6, 2024; Accepted August 13, 2024)

Keywords: Hybrid material, Spinel ferrites, Polypyrrole, Sol-gel method, Nanocomposites spherical

1. Introduction

The investigation of hybrid materials has emerged as a prominent area of scientific inquiry, driven by the imperative to identify novel materials with enhanced efficiency. These hybrid materials offer a promising approach, exhibiting superior adjustable properties, including surface modification and enhanced stability, in comparison to their individual components.[1] Spinel ferrites are ferrimagnetic materials that exhibit high resistivity, good magnetization, and excellent chemical stability.[2] They also exhibit interesting dielectric and magnetic properties, which render them particularly effective microwave absorbers.[3,4] The unit cell of ferrite is constituted by 32 oxygen anions arranged in a cubic pattern, with metal cations distributed in tetrahedral A and octahedral B sites.[5]

The properties of these ferrite crystals are dependent upon the types of cations and their distribution in sites A and B.[6]

Spinel ferrites represent an excellent option for the syntheses of hybrid materials. The synthesis of ferrite nanoparticles can be achieved through a range of methods, including sol-gel[7], co-precipitation[8], sonochemistry[9], and hydrothermal[10]. Spinel ferrites are particularly well-suited for the elaboration of hybrid materials. However, the electronic conductivity of bare spinel ferrite tends to be relatively low. This efficiency could be enhanced through the introduction of substitutions or combinations. The formation of binary hybrids with improved electrochemical properties is achievable through the combination of spinel ferrites with polymers. This is a principal attribute required for the conduction in polymers. Spinel ferrites have been combined with polypyrrole (PPy) to create nanocomposites. These nanocomposites have a granular structure and exhibit both magnetic and dielectric properties[11]. To illustrate, the in-situ polymerization method has been shown to yield hybrid $MgFe_2O_4$/polypyrrole materials that consistently demonstrate excellent electrochemical performance.[12] Moreover, the study investigates the fabrication of PPy coatings on hollow $MgFe_2O_4$ double-shell nanospheres with the objective of developing electronic

* Corresponding author: momath.lo@ucad.edu.sn
https://doi.org/10.15251/DJNB.2024.193.1215

cells and enhancing conductivity and cycling stability. The mixed ferrite spinels of $MgFe_2O_4$ when combined with PPy display low coercivity and saturation magnetization values, which suggests their potential utilization in transformer cores and switching applications. The objective of the research is to investigate the impact of doping spinel ferrite with zinc (Zn) on its potential for utilization in industrial applications. Nevertheless, the introduction of zinc ions into the spinel ferrite structure does not result in any alteration to the electrochemical behavior. Furthermore, the incorporation of Zn results in the displacement of Fe^{3+} from the tetrahedral sites to the octahedral sites, thereby enhancing the electrical performance of the resulting compounds[12]. Consequently, a variety of ferrite-doped spinel-based polypyrrole nanocomposites are extensively prepared. Nevertheless, research on polypyrrole-coated Zn-Mg ferrite spinel-like composites can be considered to be relatively limited.

This study presents a two-step procedure for synthesising new polymers based on Zn-Mg spinel ferrite ($Zn_xMg_{1-x}Fe_2O_4$) coated with polypyrrole. In the initial stage of the procedure, spinel ferrites $Zn_xMg_{1-x}Fe_2O_4$ (x = 0, 0.3) were synthesised using the sol-gel method. In the second step, polypyrrole (PPy) was generated on the surface of the $Zn_xMg_{1-x}Fe_2O_4$ spinel ferrite ($Zn_xMg_{1-x}Fe_2O_4$@PPy) through in-situ pyrrole polymerization. A comprehensive investigation was conducted using X-ray diffraction (XRD), scanning electron microscopy (SEM), energy-dispersive X-ray spectroscopy (EDS), and Fourier transform infrared (FT-IR) analyses to examine the structure, morphology, and electrochemical behavior of $Zn_xMg_{1-x}Fe_2O_4$@PPy in order to provide a detailed understanding of these properties.

2. Experimental

2.1. Materials and methods

Zinc sulfate heptahydrate $ZnSO_4.7H_2O$ (solid), iron sulfate heptahydrate $FeSO_4.7H_2O$ (solid), Magnesiumsulfate heptahydrate $MgSO_4.7H_20$ (solid), citric acid monohydrate $C_6H_8O_7.H_2O$ (solid), Iron (III) chloride anhydrous $FeCl_3$ (solid), Pyrrole (98% liquid), Ethanol (99%, liquid) were used. All products were supplied by Sigma Aldrich. Fourier transform infrared spectroscopy (FT-IR) was performed using a Magna 860 FT-IR thermoelectronic spectrometer with dry compound samples in KBr pellets. The FT-IR was used to identifythe vibrations of the different bonds as well as the compounds structures. The obtained powder phases were identified using an X-ray diffractometer (D8 Discover diffractometer in Bragg Brentano geometry equippedwith a Cu Sealed tube $\lambda k\alpha 1$ = 1.54059 Å, a quartz front monochromator, a motorized anti-scatter screen, and an energy-resolved Lynxeye XE-T linear detector). Furthermore, the width of the peaks and the size of the crystallites were determined using the aforementioned apparatus. The morphology of the powders was studied using scanning electron microscopy (SEM) at varying magnifications. The SEM images were recorded using a JOEL 6700F microscope, which features a Field Emission Gun. The images were obtained using an applied voltage of 3 kV. The qualitative composition analysis of the synthesised compounds was performed using energy-dispersive spectroscopy (EDS) characterization. The EDS analysis was conducted at an accelerating voltage of 15 kV using a Bruker Advance apparatus.

2.2. General procedure

The stoichiometric proportions of zinc sulfate heptahydrate ($ZnSO_4.7H_2O$), iron sulfate heptahydrate ($FeSO_4.7H_2O$), magnesium sulfate heptahydrate ($MgSO_4.7H_2O$), and citric acid monohydrate ($C_6H_8O_7.H_2O$) in a 1:2:3 ratio are dissolved in ethanol (150 mL). The homogeneous solution was subjected to thermal agitation at temperatures between 70 and 85 degrees Celsius for a period of approximately four hours, resulting in the formation of a viscous liquid (gel). Subsequently, the gel is subjected to a 16-hour drying process at 100 °C in an oven to eliminate any residual moisture. The resulting precursor is then ground and subjected to calcination in an electric furnace at 500 °C for four hours in the presence of air, with a heating rate of 5 °C/min.

The process is described by the following chemical reactions (1 and 2):

$$MgSO_4.7H_20 + 2FeSO_4.7H_2O + 3C_6H_8O_7.H_2O + 9.5O_2 \longrightarrow MgFe_2O_4 + 1.5S_2 + 18CO_2 + 36H_20 \quad (1)$$

$$0.7MgSO_4.7H_20 + 0.3ZnSO_4.7H_2O + 0.7FeSO_4.7H_20 + 3C_6H_8O_7.7H_2O + 9.5O_2 \longrightarrow S_2 + 18CO_2 + 36H_2O \quad Zn_{0.3}Mg_{0.7}Fe_2O_4 \quad (2)$$

Scheme 1 provides a summary of the procedure for synthesising polypyrrole-based nanocomposites and spinel ferrite. This was achieved by separately dissolving 4 g of $Zn_{0.3}Mg_{0.7}Fe_2O_4$ and 4 g of $MgFe_2O_4$ in 50 mL of distilled water. Subsequently, the solutions were subjected to magnetic stirring for a period of one hour. Following a 20-minute period of stirring at room temperature, 4 g of $FeCl_3$ was added to each dispersion. Both solutions were stirred for a period of six hours, after which the resulting black solutions were filtered and then dried in an oven at 100 °C for 12 hours in order to remove any remaining water molecules. The process yielded the final composites, $Zn_{0.3}Mg_{0.7}Fe_2O_4$@PPy and $MgFe_2O_4$@PPy.

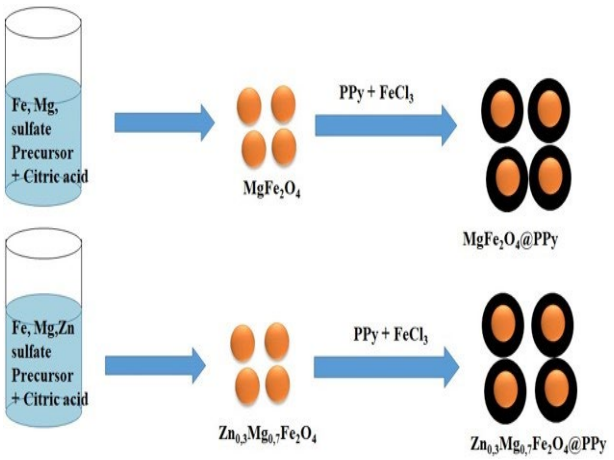

Scheme 1. Schematic illustration for the preparation of ferrite spinel. Upper panel: case of $MgFe_2O_4$ and Mg_2FO_4@PPy. Lower panel: case of $Zn_{0.3}Mg_{0.7}Fe_2O_4$ and Mg_2FO_4@PPy.

2.3. Electrochemical characterization of hybrid material

In order to investigate the electrochemical performance, the synthesised materials were deposited onto copper plate electrodes measuring 1 cm x 1 cm. The electroactivity of the synthesised materials was determined through the utilization of cyclic voltammetry. A homogeneous mixture was obtained by grinding 95% of the synthesised compounds, which served as the active material, with 5% Teflon binder in a mortar. The resulting mixture was then dispersed in a solvent (water + ethanol) to form a slurry, which was coated onto a copper plate and dried at 60 °C. Electrochemical studies, including cyclic voltammetry, were conducted using the Metrohm DropSens electrochemical workstation. An electrochemical cell was constructed with a fabricated electrode acting as the working electrode, platinum as the counter electrode, and Ag/AgCl as the reference electrode, with 1M KOH electrolyte. The active surface area of the two electrodes was calculated using the Randles–Sevcik equation (3).[13]

$$I_p = 2.69.10^5\, n^{3/2} \times A \times D^{1/2} V^{1/2} \times C_0 \quad (3)$$

Ip is the peak anodic current, A is the Active surface, D is the diffusion coefficient of the species involved in redox reactions, C_o is the concentration of redox probe, V the Scan rate, N is the number of electrons transferred in the redox reaction, D is the diffusion coefficient (D= 1.3 × 10^{-7} cm/s^2 at 25°C).

Ip represents the peak anodic current, A denotes the active surface, D corresponds to the diffusion coefficient of the species engaged in redox reactions (D= 1.3 × 10^{-7} cm/s² at 25°C), C_0 is the concentration of the redox probe, V is the scan rate, n is the number of electrons involved in the redox reaction.

3. Results and discussion

3.1 FT-IR analysis

FT-IR spectroscopy is used to identify the functional groups present in the ferrite compounds and thenanocomposites formed. The wave number range used is from 4000 to 400 cm^{-1}. Figure 1 illustrates the FT-IR spectra of $MgFe_2O_4$ and $Zn_{0.3}Mg_{0.7}Fe_2O_4$, as well as the polymerized forms $MgFe_2O_4$@PPy and $Zn_{0.3}Mg_{0.7}Fe_2O_4$@PPy. The FT-IR spectra display bands below 1000 cm^{-1} that are attributed to M-O (metal-oxygen) bonds. The presence of elongation vibration peaks at 424 and 570 cm^{-1} is indicative of the presence of Mg-O and Fe-O bonds, respectively.[14] The absorption band observed at approximately 557 cm^{-1} may be attributed to the stretching vibrations of the Zn-O and Fe-O bonds in a tetrahedral configuration.[15,16] The bands observed at 430–470 cm^{-1} are indicative of the presence of Fe–O bonds in octahedral positions. This evidence corroborates the hypothesis that the spinel structure contains both tetrahedral and octahedral ligand sites.[17,18] The broad band absorption peak observed at 3400-3500 cm^{-1} is attributed to the presence of O-H groups.[19] The bands situated between 1630 and 1650 cm^{-1} are attributed to C-O elongation.[20] The peak observed at 1554 cm^{-1} corresponds to the C-C stretching vibration of thepolypyrrole.[21] The peaks observed at approximately 1050 cm^{-1} are attributed to the in-plane deformationof the C-H and N-H bonds of the pyrrole ring. The data corroborate the formation of the synthesised compounds and the reverse or mixed oxide structure, as well as the observations made through the EDS. The presence of characteristic bands of PPy and oxides ($MgFe_2O_4$, $Zn_{0.3}Mg_{0.7}Fe_2O_4$), along with a slight shift in these bands in the composite, provides confirmation of the interfacial interaction between PPy and the oxides that occurs during composite formation. This interaction may be attributed to the binding of oxygen ions from the oxides with nitrogen atoms from the PPy macromolecules.[22]

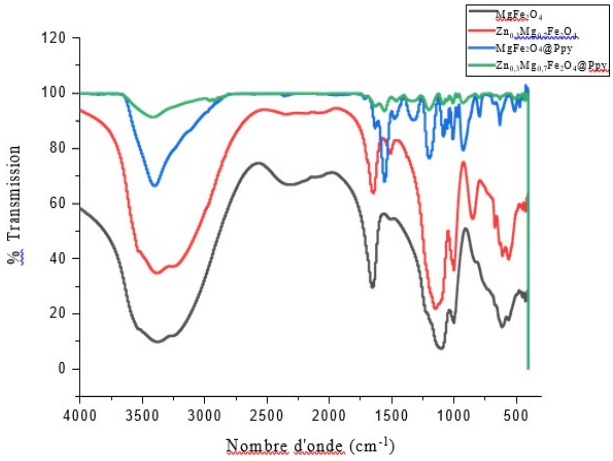

Fig. 1. FT-IR spectra of oxide spinels A) MgFe2O4, B) Zn0.3Mg0.7Fe2O4 and composites C) MgFe2O4@PPy, D) Zn0.3Mg0.7Fe2O4@PPy.

3.2. EDS analysis

The qualitative composition of the samples was analyzed using EDS characterization. Figures 2, 3, 4 and 5 illustrate the EDS spectra of the synthesised compounds. The presented spectra indicate the presence of the various elements that constitute the compounds, along with their respective percentages. The composite EDS analysis revealed the presence of characteristic peaks

for the primary elements analysed, including oxygen (O), magnesium (Mg), iron (Fe), zinc (Zn), nitrogen (N), carbon (C), and chlorine (Cl), among others[23].The presence of polypyrrole in the nanocomposites is corroborated by the N and Cl peaks observed in Figures 5 and 6. Furthermore, the data indicates the formation of both spinel oxides and nanocomposites.

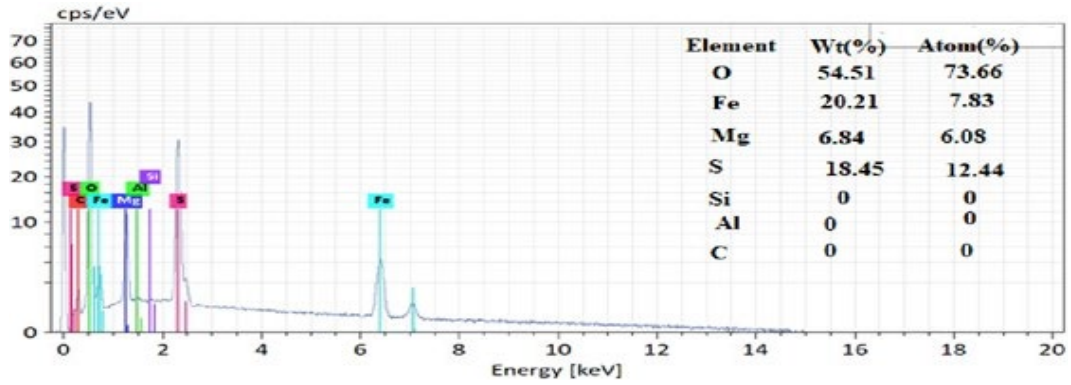

Fig. 2. EDS Spectrum of $MgFe_2O_4$.

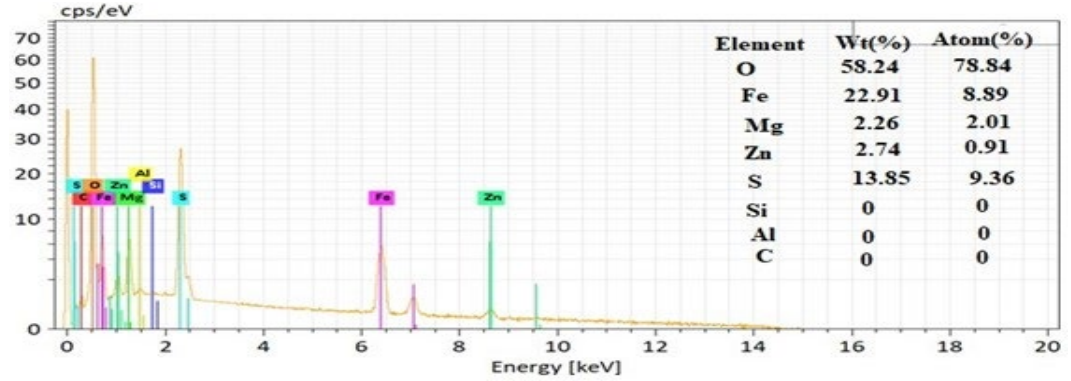

Fig. 3. EDS spectrum of $Zn_{0.3}Mg_{0.7}Fe_2O_4$.

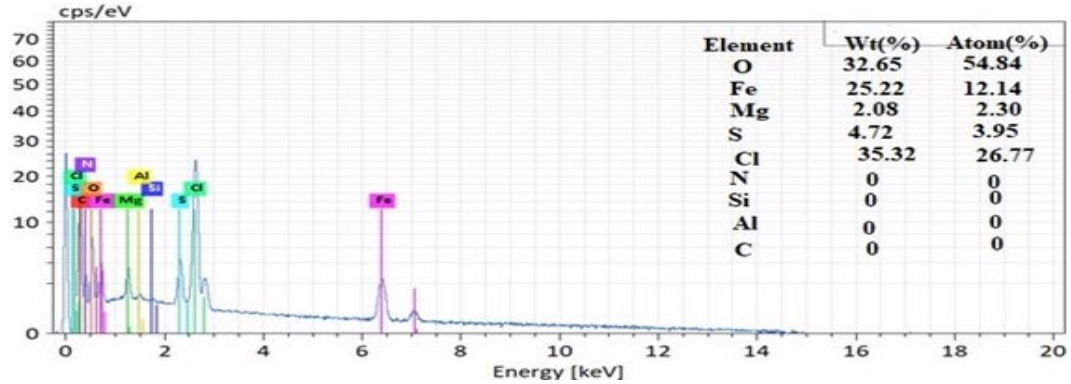

Fig. 4. EDS spectrum of $MgFe_2O_4$@PPy.

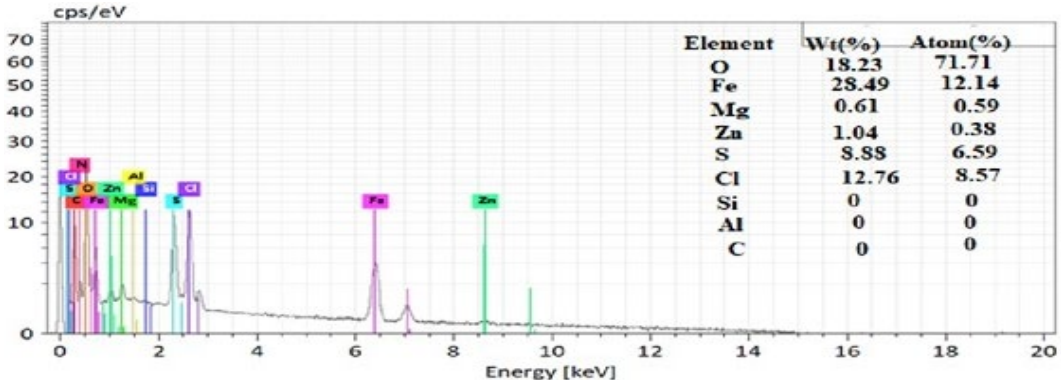

Fig. 5. EDS spectrum of $Zn_{0.3}Mg_{0.7}Fe_2O_4$@PPy

3.3. XRD analysis

Figure 6 illustrates the X-ray diffraction (XRD) spectra of the synthesised compounds, namely $MgFe_2O_4$, $Zn_{0.3}Mg_{0.7}Fe_2O_4$, $MgFe_2O_4$@PPy and $Zn_{0.3}Mg_{0.7}Fe_2O_4$@PPy. The spectra display diffraction peaks of varying intensity at angular values of 2θ = 18°, 30°, 35.5°, 37.05°, 43.42°, 53.5°, 57.34° and 62.1°.[24,25]

The peaks that correspond to the (111), (220), (311), (222), (400), (422), (511) and (440) planes, respectively, indicate the cubic and face-centred type $MgFe_2O_4$ structure, as defined by JCPDS no. 71-1232.[26] This structure is characterized by a single-phase spinel structure of space group Fd3m.[27] The intensity of the peaks is observed to decrease consistently in the polymerized form. This is presumably due to the amorphous nature of the polymer within the nanoparticle. Additionally, a change in angle was observed in the polymerized form, indicating an interaction between the different entities.

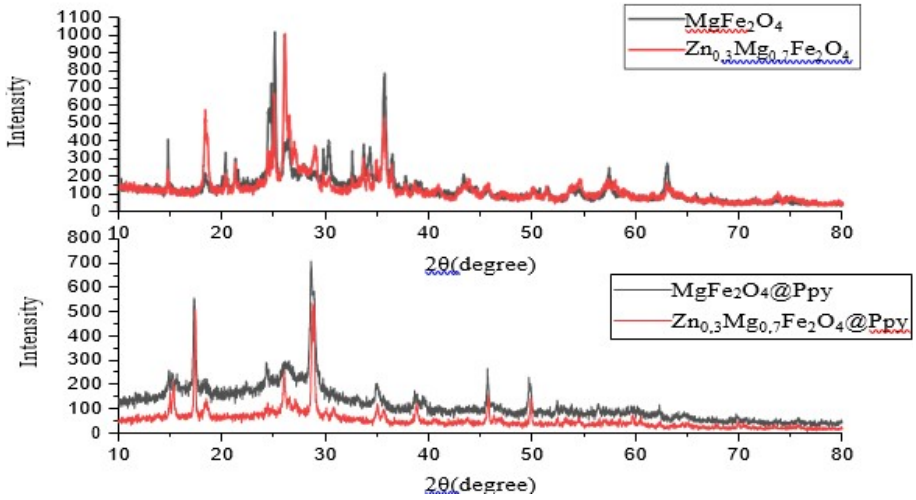

Fig. 6. XRD Spectra of the different compounds.

3.4. SEM analysis

Scanning electron microscopy (SEM) was used to analyze the surface morphology and elemental composition of the prepared samples. Fig. 7 illustrates the morphology of spinel powders synthesized with and without polymerization. The observation reveals a uniform distribution of grains with varying shapes (spherical and elliptical) and sizes.[29]

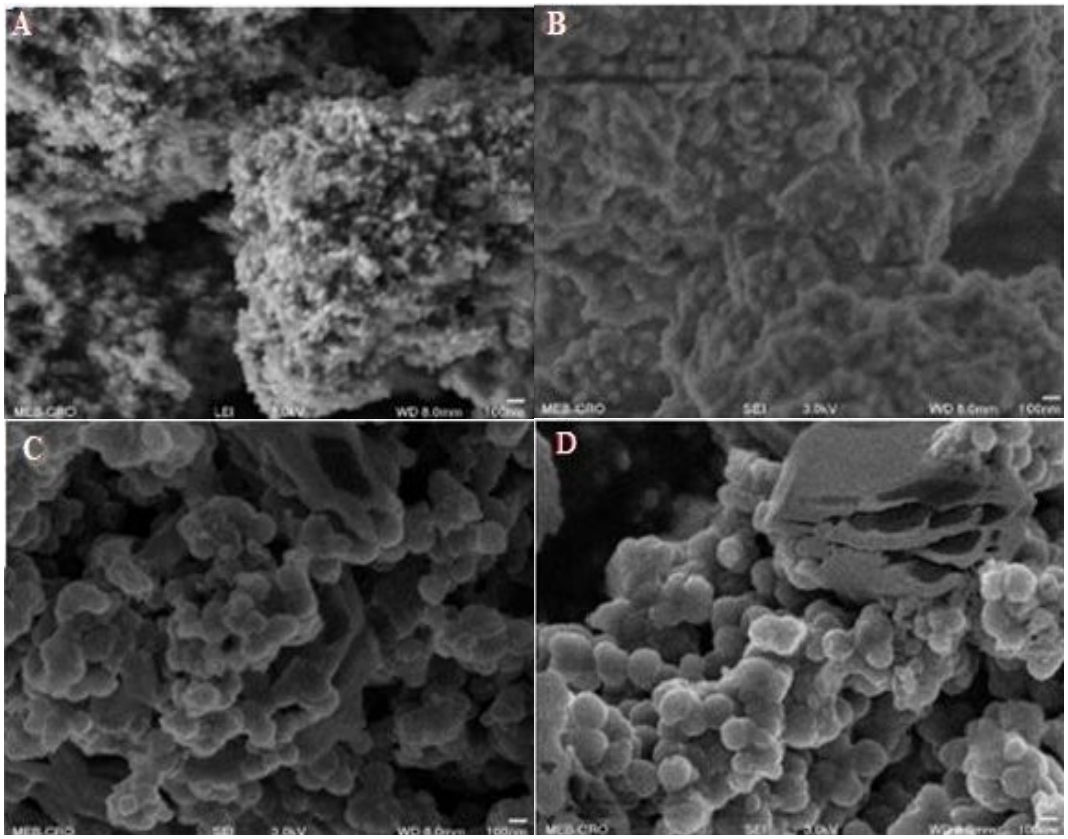

Fig. 7. SEM images of different compounds A) $MgFe_2O_4$, B) $Zn_{0.3}Mg_{0.7}Fe_2O_4$, C) $MgFe_2O_4$@PPy and D) $Zn_{0.3}Mg_{0.7}Fe_2O_4$@PPy.

The presence of agglomerated grains in photographs A and B is attributed to the ferromagnetism of the ferrite $MgFe_2O_4$ and $Zn_{0.3}Mg_{0.7}Fe_2O_4$,, respectively, as well as the existence of porous cavities at the nanometric scale.[30] SEM images of MgFe2O4 and Zn0.3Mg0.7Fe2O4 coated with PPy are shown in photographs C and D, respectively. The coatings were formed through oxidative polymerization. The SEM images provide further evidence that the nanospheres are homogeneous and can be individually identified with a nanoscale width. As illustrated in the figures, the SEM images of PPy on $MgFe_2O_4$ and on $Zn_{0.3}Mg_{0.7}Fe_2O_4$ indicate that the arrangement of the ferrite spinels remains unaltered. Instead, the PPy gradually wraps around the spinels in a sequential manner. It is notable that the PPy deposit is confined to the spherical walls, resulting in strong interactions between the PPy and the ferrite spinels.

3.5. Electrochemical characterization of the different synthesized compounds

Figure 8 provides an illustration of the electrochemical response (CV) of electrodes prepared with the aforementioned compounds. The cyclic voltammetry (CV) was recorded at a scan rate of 50 mV/s and between the potentials of -1.2 and 0.6 V. Figures 8a and 8b illustrate voltammograms with a cathodic peak at approximately -0.6 V and -0.95 V, respectively. This peak may be associated with the two-step reduction of Fe^{3+} to Fe. Furthermore, an anodic peak at approximately -0.35 V (see Figures 8a and 8b) may be attributed to the reversible oxidation of Fe/Fe^{3+}.[31,32] The reduction peak at -0.38 V correlates with the reduction of $MgFe_2O_4$ to MgO[34]. Additionally, doping Mg with Zn has been observed to enhance its electrical properties in comparison to $MgFe_2O_4$ (Figure 8b).[34] The CV curves display disparate trends when ferrite spinels are fully covered with PPy, as illustrated in Figures 8c and 8d. Furthermore, the current peak values have increased by 0.35. Both the $MgFe_2O_4$@PPy and $Zn_{0.3}Mg_{0.7}Fe_2O_4$@PPy compounds exhibit two oxidation peaks at approximately -3.24 V and 1.74 V. The shift in oxidation peaks in comparison to the ferrite spinels indicates the presence of a PPy coating on $MgFe_2O_4$ and $Zn_{0.3}Mg_{0.7}Fe_2O_4$[36]. When the ferrite spinels

are completely covered with PPy, two reduction peaks emerge at approximately -544 and -1016 mV for $MgFe_2O_4$@PPy and at approximately -554 and -1098 mV for $Zn_{0.3}Mg_{0.7}Fe_2O_4$@PPy, respectively (see Figures 8c and 8d). Furthermore, Table 1 illustrates that the hybrid materials $MgFe_2O_4$@PPy and $Zn_{0.3}Mg_{0.7}Fe_2O_4$@PPy exhibit higher intensities of oxidation and reduction peaks, as well as greater active surface areas. The results indicate that $Zn_{0.3}Mg_{0.7}Fe_2O_4$@PPy has the most favorable electrochemical properties, which can be attributed to the Zn doping in the ferrite matrix (as illustrated in Figure 8d). This indicates the formation of polypyrrole around the ferrite spinels $MgFe_2O_4$ and $Zn_{0.3}Mg_{0.7}Fe_2O_4$. Furthermore, the deposition of the PPy layer enhanced the conductivity of the ferrite spinels, thereby facilitating the formation of PPy nanospheres.

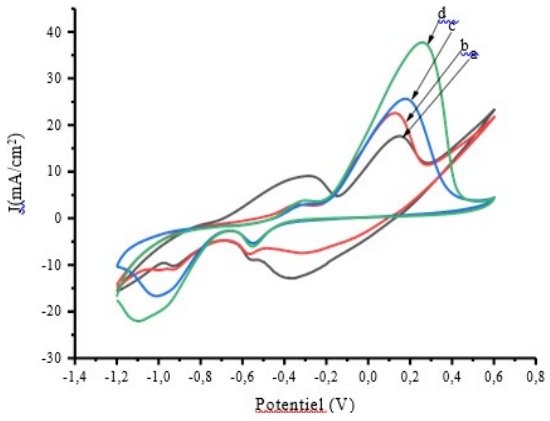

Fig. 8. Cyclic Voltammetry of different compounds with 50 mV.s^{-1} scan rate in 1M KOH electrolyte: a) $MgFe_2O_4$, b) $Zn_{0.3}Mg_{0.7}Fe_2O_4$, c) $MgFe_2O_4$@PPy and d) $Zn_{0.3}Mg_{0.7}Fe_2O_4$@PPy.

Table 1. Kinetic characterization of cyclic voltammetry of different composites at 50 mV/s scan rate.

Nanocomposites	[a]Eox(mV)		[b]Ered(mV)			[c]Ja(mA/cm^2)		[d]Jc (mA/cm^2)			[e]Sac(cm^2)
$MgFe_2O_4$	-288	144	-932	-566	-378	8.9	17.45	-10.41	-8.97	-13.01	0.14
$Zn_{0.3}Mg_{0.7}Fe_2O_4$	-364	120	-922	-560	-310	2.57	22.39	-11.09	-9.07	-7.62	0.18
$MgFe_2O_4$@PPy	-324	174	-544	-1016		2.62	25.46	-5.49	-	16.86	0.2
$Zn_{0.3}Mg_{0.7}Fe_2O_4$@PPy	-318	258	-554	-1098		3.52	37.59	-6.22	-	22.26	0.306

[a]Eox = oxidation potential, [b]Ered = reduction potential, [c]Ja = anodic current intensity, [d]Jc = cathodic current intensity, [e]Sac = active surface

The influence of the scan rate on the 1M KOH electrolyte was examined. Cyclic voltammetry data were collected for a series of electrode samples of varying compounds at scan rates between 30 and 80 mV/s, with an increment of 10 mV/s (see figures A, B, C, and D). The measurements were conducted within the potential range of -1.2 to 0.6 volts with respect to a silver/silver chloride reference electrode. The CV curves indicate a gradual increase in current under the curve with an increase in scan rate, which suggests that the voltammetric current is directly proportional to the scan rate. Furthermore, the peak current is observed to increase with the scan rate, indicating that the rates of electronic and ionic transport are sufficiently rapid at the applied scan rates.[37] It can be observed that an increase in the scan rate does not result in a notable alteration to the shape of the cyclic voltammetry curves. This suggests that there is an enhancement in electron conduction within the host materials. Furthermore, elevated scan rates result in a shift of the anodic and cathodic peaks towards higher and lower potentials, respectively.[35] In figures 9, 10, 11 and 12, the peaks labelled A', B' and C' represent the three reduction processes. The oxidation peaks A and B are in correspondence with the reduction peaks A' and B'. It can be observed that the oxidation peaks A and B are reversible reaction processes, while the reduction peak C is an irreversible process.[38,33]

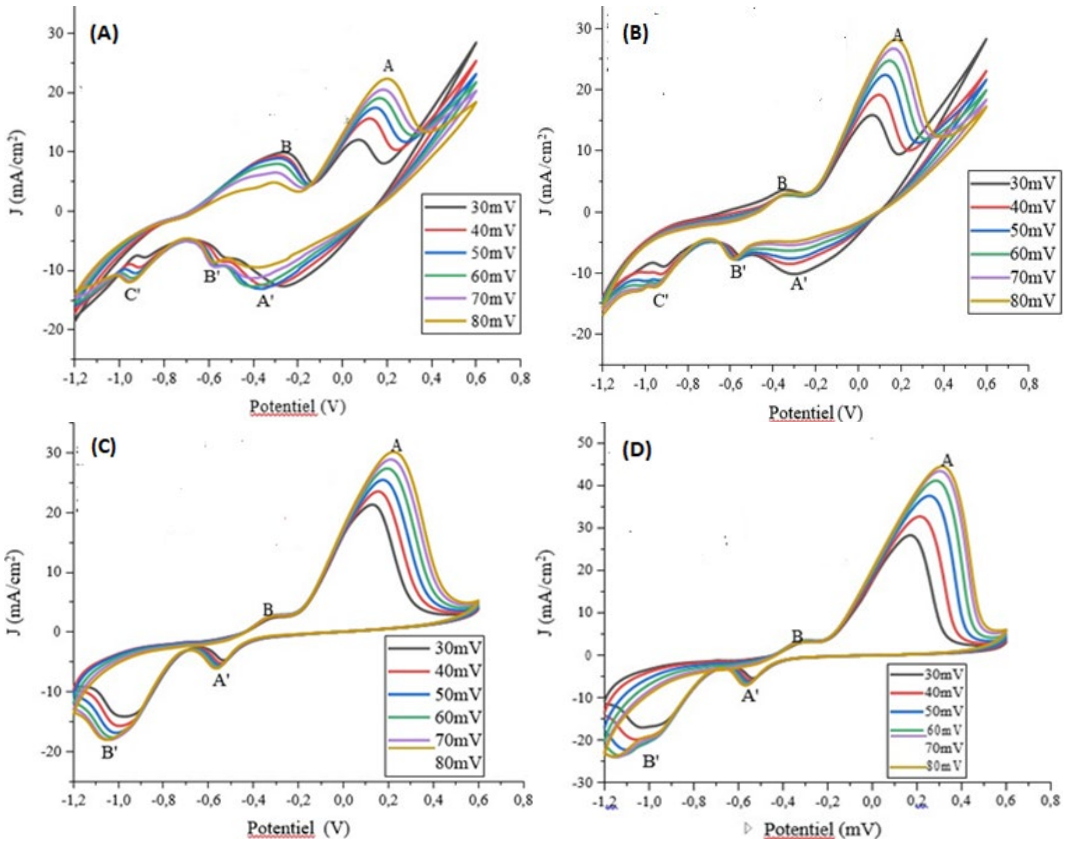

Fig. 9. Cyclic Voltammetry of at different scan rates in 1M KOH electrolyte A) $MgFe_2O_4$ B) $Zn_{0.3}Mg_{0.7}Fe_2O_4$ C) MgFe2O4@PPy and D) $Zn_{0.3}Mg_{0.7}Fe_2O_4$@PPy.

The relationship between the anodic and cathodic peaks demonstrates a linear increase with the square root of the sweep speed, indicating that the redox reactions of different composites are occurring rapidly in the electrodes. Consequently, the electrochemical reactions of the various peaks can be classified as diffusion-controlled reactions.[39]

4. Conclusion

Spinel oxides were synthesised via the sol-gel method and subsequently polymerised through chemical oxidative polymerization, resulting in the formation of nanocomposites. The results of the X-ray diffraction (XRD), energy dispersive spectroscopy (EDS), scanning electron microscopy (SEM) and Fourier transform infrared spectroscopy (FT-IR) spectroscopic methods provided confirmation of the formation of oxides and nanocomposites. The XRD and FT-IR results indicate that all the spinels possess a cubic structure. Furthermore, the interaction between the oxide and pyrrole is based on the formation of hydrogen bonds and electrostatic interactions between the different entities.

The application of scanning electron microscopy (SEM) revealed a uniform distribution of the nanocomposites. The EDS analysis corroborated the presence of the characteristic peaks of these compounds and confirmed the observed 1:2 ratio between Mg and Fe. Voltammograms demonstrated that the polymerised forms exhibited enhanced conductivity compared to the mixed oxides alone.

This work illustrates the significance of polymers in enhancing the conductivity of ferrite spinels without modifying their configuration. Furthermore, the possibility of constructing hybrid materials through the interaction between PPy and ferrite spinels is demonstrated. These ferrite spinels can be employed as a model for the in-situ electrodeposition of polypyrrole nanocomposites, which results in the formation of polymers with notable electrochemical properties.

Acknowledgments

The authors would like to express their gratitude to Christophe Lefevre, Leuvrey Cédric, and Marc Lenertz from IPCMS, University of Strasbourg, for their assistance in conducting the necessary FT-IR, XRD, EDS, and SEM measurements.

References

[1] R. M. Khafagy, Journal of Alloys and Compounds, **509**(41) 9849(2011); https://doi.org/10.1016/j.jallcom.2011.07.008

[2] Y. Yang, L. Liu, H. Zhu, N. Bao, J. Ding, J. Chen, K. Yu, ACS Applied Materials Interfaces. **12**(14) 16609 (2020); https://doi.org/10.1021/acsami.0c00920

[3] P. Gairola, L. P. Purohit, S. P. Gairola, P. Bhardwaj, S. Kaushik, Progress in Natural Science: Materials International, **29**(2) 170 (2019); https://doi.org/10.1016/j.pnsc.2019.03.011

[4] H. Arabi, N. K. Moghadam, Journal of Magnetism and Magnetic Materials, **335**(2) 144 (2013); https://doi.org/10.1016/j.jmmm.2013.02.006

[5] I. Chihi, M. Baazaoui, N. Hamdaoui, J. M. Greneche, M. Oumezzine, K. Farah, Journal of Materials Science: Materials in Electronics, **32**(12) 16634 (2021); https://doi.org/10.1007/s10854-021-06218-5

[6] M. Amiri, M. Salavati-Niasari, A. Akbari, Advances in Colloid and Interface Science 265(1), 29 (2019); https://doi.org/10.1016/j.cis.2019.01.003

[7] J. C. R. Araújo, S. Araujo-Barbosa, A. L. R. Souza, C. A. M. Iglesias, J. Xavier, P. B. Souza, F. Bohn, Journal of Physics and Chemistry of Solids, 154, 110051 (2021); 110051; https://doi.org/10.1016/j.jpcs.2021.110051

[8] T., A, A. Ajeesha, M. George, A. Manikandan, J. A. Mary, Y. Slimani, A. Baykal, Physica B: Condensed Matter, 606, 412660 (2020); https://doi.org/10.1016/j.physb.2020.412660

[9] Y. Shen, Y. Wu, X. Li, Q. Zhao & Y. Hou. One-pot synthesis of MgFe2O4 nanospheres by solvothermal method. Materials Letters, 96, 85 (2013); https://doi.org/10.1016/j.matlet.2013.01.023

[10] N.A. Ali, N.H. Idris, M.F.M. Din, N.S. Mustafa, N.A. Sazelee, F.A.H. Yap, N.N. Sulaiman, M.S. Yahya, M. Ismail,.. RSC Adv, 8 (3), 15667 (2018); https://doi.org/10.1039/C8RA02168F

[11] W. Fan, M. Li, H. Bai, D. Xu, C. Chen, C. Li, Y. Ge, W. Shi, Langmuir 32 (6) 1629 (2016); https://doi.org/10.1021/acs.langmuir.5b03887

[12] G. Li, S. Yan, E. Zhouc, Y. Chena, Colloids and Surfaces A: Physicochemical and Engineering Aspects, 276(3), 40 (2006); https://doi.org/10.1016/j.colsurfa.2005.10.010

[13] P. Karthikeyan, S. S. Elanchezhiyan, S. Meenakshi C. M. Park, Journal of Hazardous Materials, 408 124892 (2021); https://doi.org/10.1016/j.jhazmat.2020.124892

[14] R. R. Powar, V. D. Phadtare, V. G. Parale, S. Pathak, K. R. Sanadi, H.-H. Park, D. N. Zambare, Materials Science and Engineering: B, 262, 114776 (2020); https://doi.org/10.1016/j.mseb.2020.114776

[14] L. Bai, R. Yuan, Y. Chai, Y. Yuan, Y. Wang, S. Xie, Chemical Communications, 48(89), 10972 (2012); https://doi.org/10.1039/c2cc35295h

[15] A.V. Anupama, V. Rathod, V.M. Jali, B. Sahoo, Composition dependent elastic and thermal properties of Li-Zn ferrites, Journal of Alloys and Compound, 728 1091 (2017);

https://doi.org/10.1016/j.jallcom.2017.09.099
[16] Z. Varzi, A. Maleki, Applied Organometallic Chemistry, 33(8) e5008 (2019); https://doi.org/10.1002/aoc.5008
[17] A. Manohar, C. Krishnamoorthi, Journal of Photochemistry and Photobiology B: Biology, 173 456 (2017); https://doi.org/10.1016/j.jphotobiol.2017.06.025
[18] J. Li, D. H. L. Ng, P. Song, Y. Song, C. Kong, Journal of Industrial and Engineering Chemistry, 23 290 (2015); https://doi.org/10.1016/j.jiec.2014.08.031
[19] K. Kombaiah, J. J. Vijaya, L. J. Kennedy, M. Bououdina, Ceramics International, 42(2) 2741 (2016); https://doi.org/10.1016/j.ceramint.2015.11.003
[20] M. Joulaei, K. Hedayati, D. Ghanbari. Composites Part B: Engineering, 176(1) 107345 (2019); https://doi.org/10.1016/j.compositesb.2019.107345
[21] K. Geetha, R. Udhayakumar, & A. Manikandan. Enhanced magnetic and photocatalytic characteristics of cerium substituted spinel MgFe2O4 ferrite nanoparticles. Physica B: Condensed Matter, 615 413083 (2021); https://doi.org/10.1016/j.physb.2021.413083
[22] H. Yuvaraj, M.H. Woo, E.J. Park, Y.T. Jeong, K.T. Lim, European Polymer Journal 44 637 (2008); https://doi.org/10.1016/j.eurpolymj.2008.01.007
[23] J. Jiang, L. Ai, L. Li, Journal of Physical Chemical B, 113 1376 (2009); https://doi.org/10.1021/jp808270n
[24] S, Nasirian, HM .Moghaddam. Polymer, 55 1866 (2014); https://doi.org/10.1016/j.polymer.2014.02.030
[24] J. Zhang, M. Yan, G. Sun, X. Li & K. Liu, Journal of Alloys and Compounds, 889 161673(2022); https://doi.org/10.1016/j.jallcom.2021.161673
[25] P. Prajapat, S. Dhaka, & H. S. Mund, Journal of Electronic Materials, 50(8) 4671 (2021); https://doi.org/10.1007/s11664-021-09022-3
[26] J. Zhao, T. Wang, X. Liu, X. Kan, C. Liu, W. Wang, M. Shazeda, Journal of Materials Science: Materials in Electronics, 32(4), 4008 (2021); https://doi.org/10.1007/s10854-020-05143-3
[27] J.P. Dhal, S.K. Sahoo, B.G. Mishra, G. Hota, Material Letter, 196, 95 (2017); https://doi.org/10.1016/j.matlet.2017.02.118
[28] S.K. Durrani, S. Naz, M. Mehmood, M. Nadeem, M. Siddique, Journal of Saudi Chemical Society 21 (8), (2017) 899-910; https://doi.org/10.1016/j.jscs.2015.12.006
[29] R. Qindeel, & N. H. Alonizan, Materials Science and Engineering: B, 244, 43 (2019); https://doi.org/10.1016/j.mseb.2019.04.022
[30] J. Husain, N. Reddy, A. Begum, S. Farheen, S. M. Nayak, G. Shivaraj, D. Pathar, Materials Today: Proceedings, 46 410 (2021); https://doi.org/10.1016/j.matpr.2020.09.338
[31] Z. Hammache, A. Soukeur, S. Omeiri, B. Bellal, M. Trari, Journal of Materials Science: Materials in Electronics. 30, 5375 (2019); https://doi.org/10.1007/s10854-019-00830-2
[32] Z. Bazhan, F. E. Ghodsi, J. Mazloom, Electrochimica Acta, 250, 143 (2017); https://doi.org/10.1016/j.electacta.2017.08.026
[33] L. Chang , L. Jinglong, L. Hui , Y. Hongyan, Z. Sijia, C. Weigang and L. Wang. Crystals 11, 925 (2021)
[34] K. Ahmad, S. M. Mobin, Nanoscale Advances, 1, 719 (2019); https://doi.org/10.1039/C8NA00007G
[35] H.M. Zaki, S. Al-Heniti, A. Umar, F. Al-Marzouki, A. Abdel-Daiem, T.A. Elmosalami, H.A. Dawoud, F.S. Al-Hazmi, S.S. Ata-Allah, Journal of Nanoscience Nanotechnology, 13 (6) 4056 (2013); https://doi.org/10.1166/jnn.2013.7434
[36] X. Zhao, Y. Jiao, P. Xue, M. Feng, Y. Wang, Z. Sha, ACS Sustainable Chemistry Engineering, 8 (12), 4827 (2020); https://doi.org/10.1021/acssuschemeng.9b07644

[37]Y. Zhang, M. Ma, J. Yang, C. Sun, H. Su, W. Huang, X. Dong, Nanoscale, 6 (16), 9824 (2014); https://doi.org/10.1039/C4NR02833C

[38] D. Guo, H. Zhang, X. Yu, M. Zhang, P. Zhang, Q. Li, T. Wang, Journal of Materials Chemistry A, 1(24), 7247 (2013); https://doi.org/10.1039/c3ta10909g

[39] S. Vandarkuzhal, N. Gogoi, S. Ghosh, B. Prabhakara Reddy, K. Nagarajan,. Electrochimica Acta, 59, 245 (2012); https://doi.org/10.1016/j.electacta.2011.10.062